Supplement Information (SI Appendix)

The Charged Linker of the molecular chaperone Hsp90 modulates domain contacts and biological function.

Markus Jahn, Alexandra Rehn, Benjamin Pelz, Björn Hellenkamp, Klaus Richter, Matthias Rief, Johannes Buchner, and Thorsten Hugel

Methods

Molecular Cloning

All Hsp90 mutants were derived from yeast Hsp90 (Hsp82) and numbering refers to the amino acid sequence of yeast Hsp90 wild type (WT).

Constructs for Optical Tweezers and *in vitro* experiments

To obtain the full unfolding pattern of Hsp90 in optical tweezers, WT Hsp90 was genetically inserted between two ubiquitin domains (WT-diUbi) (Figure 1A). The C-terminal ubiquitin was fused to a His-Tag. The mechanically stable ubiquitins serve as spacers and carry cysteine mutations for DNA handle coupling. For details see (1, 2).

Constructs used for charged linker (CL) characterization in optical trap experiments (WT-cys, Sub211-263, Sub211-272, WT-ΔMC and WT-ΔN) and *in vitro* assays were expressed as an N-terminally His-tagged SUMO (Small Ubiquitin-related Modifier) fusion protein followed by the respective Hsp90 mutant. SENP protease (sentrin-specific protease) was used to cleave C-terminal peptides from SUMO, leaving a tag free Hsp90 mutant (3).

DNA of constructs WT, Sub211-263 and Sub211-272 was synthesized by Life Technologies (Darmstadt, Germany) and sub-cloned into pET28 vector (Novagen, Germany). In Sub211-263 and Sub211-272 the respective amino acid (aa) regions were substituted by glycine-glycine-serine (GGS) repeats of the same length. Both substitution constructs have two cysteine mutations D61C and D560C. WT_cys was derived from WT inserting the same cysteine mutations by Quikchange Lighting (Agilent Technologies, USA). In the main text we use WT instead of WT_cys for better comprehensibility.

Deletion constructs WT-ΔMC and WT-ΔN were derived from WT by genetically deleting aa 281 to 709 and aa 1 to 178 respectively with Phusion Kit (New England Biolab, USA). WT-ΔMC has two cysteine mutations at amino acid positions 3 and 278. WT-ΔN has two cysteine mutations at amino acid positions 183 and 560. All point mutations were introduced by Quikchange Lighting (Agilent Technologies, USA).

Constructs for FRET experiments

For FRET experiments Hsp90s with an N-terminal His-Tag and a C-terminal coiled-coil motif followed by a Strep-tag (used for purification) were used (WTzip) as described in (4). Substitution mutants (Sub211-263zip and Sub211-272zip) were engineered by cloning of the substitution regions from Sub211-263 and Sub211-272 into WTzip. To couple dyes, cysteine mutations were introduced at position 61 for donor molecules and at position 385 for acceptor molecules. In the main text (fluorescence and crosslinking section) we omit “zip” and use WT, Sub211-263 and Sub211-272 for better comprehensibility.

Protein Expression and Purification

For protein expression, the Hsp90 containing plasmids were transformed in BL21DE3 cod+ (Stratagene, USA). Proteins were expressed overnight at 20°C. Cells were harvested by centrifugation, resuspended in loading buffer (100 mM sodium phosphate, 300 mM NaCl, 20 mM imidazole, pH 8) and lysed in a French Press (Constant Systems, UK).

His-tagged proteins were loaded onto a Ni-NTA tag column (GE Healthcare, USA), washed and eluted by a linear gradient with elution buffer (100 mM sodium phosphate, 300 mM NaCl, 500 mM imidazole, pH 8). If the construct carried a SUMO tag it was digested over night with SENP during dialysis to loading buffer at 4°C and additionally purified on the Ni-NTA column (GE Healthcare, USA) collecting the flow-through. Strep-tagged proteins used in FRET and fluorescent experiments were purified on a Strep-Tactin Superflow column (IBA, Germany) with supplied buffers and protocols instead.

All constructs were further purified by Anion Exchange on a Mono Q column (GE Healthcare, USA) using a linear gradient between low salt and high salt buffer (40 mM Hepes, 50 mM / 1 M NaCl, 1 mM TCEP, pH 7.5) followed by a size exclusion column Superdex 200 (GE Healthcare, USA) in 40 mM Hepes, 200 mM KCl, 1 mM TCEP, pH 7.5. Protein purity was determined by SDS-PAGE, aliquots were frozen in liquid nitrogen and stored at -80°C.

Cochaperones were purified as previously described (5, 6).

Optical Tweezers Setup & Procedures

Setup

The experimental setup used for optical trapping is a custom-built high-resolution dual trap optical tweezers with back-focal plane detection as described previously (7). Briefly, a 4W diode pumped Nd:YVO4 solid state laser (Spectra-Physics, USA) is split into its two polarization directions. One of the beams can be deflected by a piezo mirror stage (Mad City Labs, USA), providing lateral displacement of one of the traps in the specimen plane. After recombining the beams, they are expanded to overfill the back aperture of the trapping objective (63x/1.20 W Corr, C-Apochromat, Zeiss, Germany). To monitor bead displacement the forward scattered light of the trapped beads is collected by a second identical objective and imaged onto two quadrant photodiodes (QP154-Q-HVSD, First Sensor, Germany).

Preparation of Samples

For protein DNA coupling cysteine residues were reduced with 10 mM TCEP for 15 minutes at 20°C followed by a rapid buffer exchange to phosphate buffered saline (PBS) pH 6.7. 24 bp, single stranded DNA oligos with a 3' maleimide modification (Biomers, Germany) were attached to the protein at 20°C for 1 h. Using maleimide chemistry offers an easier and faster alternative than previously used thiol oligos. Excess DNA oligos were removed using a Superdex 200 column (GE Healthcare, USA).

370 nm dsDNA handles with either biotin or digoxigenin modification at 5' and an overhang complementary to the protein coupled oligo at 3' were generated by PCR as described in (1, 8).

Measurement Procedures

Protein, DNA handles and 1 µm silica beads (Bangs Laboratories, USA), on-site functionalized with anti digoxigenin (Roche, Switzerland) and tetramethylrhodamine-BSA (Molecular Probes, USA) were incubated and diluted in measurement buffer (40 mM Hepes, 150 mM KCl, 10 mM $MgCl_2$, pH 7.4). Streptavidin coated 1 µm silica beads (Bangs Laboratories, USA) were added. The following oxygen scavenger system to avoid photo-damage was used: glucose 0.33 % (Sigma, Germany), 13 U/ml glucose oxidase (Sigma, Germany), 8500 U/ml catalase (Calbiochem, Germany), (final concentrations in measurement buffer).

One anti-digoxigenin and one streptavidin bead were caught in the laser spots and brought in close proximity. After successful single tether formation, one can repeatedly unfold the protein construct by moving the traps apart and together with constant-velocity, while measuring the displacement of the beads. Constant-distance experiments were performed by keeping the traps separated at a certain distance, while monitoring bead displacement over time.

The stiffness of each individual trap was about 0.4 pN/nm set by laser intensity and each bead pair was calibrated individually. The calibration is the major error source with a force error of about 10 %. The temperature at the position of the protein is approximately 30°C.

Data Evaluation

From the bead deflections the force was calculated using the measured trap stiffness. The extension is obtained by subtracting the beads displacements from the trap centers from the distance between the beads. To model force extension curves and extract DNA parameters and protein contour length increases we used polymer models.

The elasticity of DNA can be modelled by an extensible worm-like chain interpolation equation (eWLC) (9).

$$F_{eWLC}(x) = \frac{k_B T}{p_D}\left(\frac{1}{4\left(1-\frac{x}{L_D}+\frac{F}{K}\right)^2}-\frac{1}{4}+\frac{x}{L_D}-\frac{F}{K}\right) \qquad (1)$$

with force F, extension x, thermal energy k_BT, DNA persistence length p_D, DNA contour length L_D, elastic stretch modulus K

The force-extension relation of an unfolded amino acid chain can be described using a WLC model.

$$F_{WLC}(x) = \frac{k_B T}{p_P}\left(\frac{1}{4\left(1-\frac{x}{L_P}\right)^2} - \frac{1}{4} + \frac{x}{L_P}\right) \quad (2)$$

with protein contour length L_P, and protein persistence length p_P

Multidomain unfolding patterns were analyzed by globally fitting an eWLC in series with one or more WLC fits for each unfolding event. Protein persistence length was fixed at 0.7 nm. Fits yielded expected DNA persistence lengths of about 25 nm and DNA contour lengths of about 370 nm. To account for unfolded regions and the CL we assumed an additional contribution with the following fixed protein contour length. We presumed 28 nm for the CL and also 20 nm for unfolded regions when pulling WT-diUbi, which is mainly the unfolded C-terminus when pulling full length Hsp90.

Contour length increases from domain unfolding dL_P were transformed into numbers of amino acids n_{aa} with the length of the folded domains taken from crystal structure d_{CS} and a length per amino acid of d_{aa} = 0.365 nm.

$$n_{aa} = \frac{dL_P + d_{CS}}{d_{aa}} \quad (3)$$

The kinetics between the docked and the undocked CL state were investigated in equilibrium constant distance experiments, keeping the traps at different fixed distances while monitoring the transitions. With increasing fixed distance and thus higher average force (pretension) one can populate or depopulate the docked (or undocked) state. Due to high noise in the low force region we assigned each trajectory point using discrete Hidden Markov modelling similar to (1, 10). In short: Each trace was coarse-grained into 200 force bins. Then emission probabilities and mean force were optimized using repeatedly Forward-Backward and Baum-Welch-Algorithm keeping the transition probabilities fixed.

Populations of docked and undocked CL at different pretensions were derived dividing the sum of dwell times in one state by the total trace time.

Energies can be calculated with equilibrium statistical mechanics. The free energy stored in the system at a certain force $G(F)$ is the sum of the energy of the protein in a certain state G^0, the energy of the bead displacement in a harmonic potential $G^{bead}(F)$, the energy of the DNA linker $G^{DNA}(F) = \int_0^{x_{eWLC}(F)} F_{eWLC}(x')dx'$ (see equation 1) and the energy of the unfolded peptide $G^{unfprot}(F) = \int_0^{x_{WLC}(F)} F_{WLC}(x')dx'$ (see equation 2).

$$G(F) = G^0 + G^{bead}(F) + G^{DNA}(F) + G^{unfprot}(F) \quad (4)$$

Force dependent probabilities are related to the energy difference between docked and undocked CL states. The ratio of the probabilities for these two states is

$$\frac{P_d(F_2)}{P_u(F_1)} = \exp\left(-\frac{G_d(F_2) - G_u(F_1)}{k_B T}\right) \quad (5)$$

With probability of the docked state $P_d(F_2)$ at a certain force F_2, the probability of the undocked state $P_u(F_1)$ at the corresponding force F_1 and the energy difference $G_d(F_2) - G_u(F_1)$ of the complete system.

The energy difference was derived by a global fit to both state probabilities with this model. The probability error resulting from the finite measurement time was estimated using Monte Carlo simulation (1, 11). Errors that result from uncertainties of DNA parameters and force calibration were neglected.

Transition rates at different loads were extracted fitting dwell time histograms with single exponentials using a cut off for too rapid and thus not detected transitions. Then measured rates were corrected for missed transitions simulating the transition network as described earlier (12).

Rates at zero force for docking k_d^0 and undocking k_u^0 and the distance x_T to the transition state T were derived fitting

$$k_{d/u}(F_{d/u}) = k_{d/u}^0 e^{\left(-\frac{\Delta G^T{}_{d/u}(F_{d/u}, F_T)}{k_B T}\right)} \quad (6)$$

with the free energy (equation 4) difference of the complete system $\Delta G^T{}_{d/u}$ between docked/undocked and transition state, for details see (2). The rates at zero force are extrapolated over a small force range (less than 5 pN), which together with errors in force calibration and DNA parameters might result in an error of one order of magnitude (1).

Confocal FRET Setup & Procedures

Setup

N-terminal opening and closing was quantified using confocal single pair FRET (spFRET). FRET efficiencies of freely diffusing Hsp90 dimers were measured in a homebuilt confocal microscope similar to other published setups (13-15). Time traces of burst intensities were recorded with two single photon avalanche photodiodes (PDM-50 µm, PicoQuant, Germany)

for green and red fluorescence detection and a commercial data acquisition system (HydraHarp 400, PicoQuant, Germany). Two pulsed diode lasers (532 nm LDH-P-FA-530, PicoQuant, Germany, and 640 nm LDH-D-C-640, PicoQuant, Germany) as excitation sources and an apo 60x water immersion objective (Nikon, Japan) were used.

Preparation and Measurement Procedure

Fluorescent dyes were covalently attached to the zipped Hsp90 mutants Sub211-272zip, Sub211-263zip and WTzip by maleimide chemistry. Each CL-variant and WTzip were labeled at aa position 61 with Atto 550 and exchanged with WTzip labeled at aa position 385 with Atto 647N, as described in (16), yielding heterodimers with substituted CL in one of both monomers. Each construct was incubated with different nucleotides at room temperature for 1 hour and then measured at concentrations of about 50 pM for more than 30 minutes at approximately 23°C in measurement buffer (see optical trap preparation).

Data Evaluation

For each photon burst containing more than 50 photons stoichiometry and FRET efficiency values were calculated and correlated in a 2D-plot in order to separate the FRET events from donor only and acceptor only events (see Fig. S8B,C). FRET efficiency histograms were corrected for different detection efficiencies, different quantum efficiencies of the dyes, direct excitation of the acceptor caused by the green laser and leakage of donor fluorescence in the red channel.

The corrected FRET efficiency can be written as:

$$E = \frac{F_{Dex}^{A} - lF_{Dex}^{D} - dF_{Aex}^{A}}{F_{Dex}^{A} - lF_{Dex}^{D} - dF_{Aex}^{A} + \gamma F_{Dex}^{D}} \qquad (7)$$

with

$$\gamma = Q_A \eta_A / Q_D \eta_D \qquad (8)$$

where F_{Dex}^{A} is the acceptor fluorescence intensity A after donor excitation Dex, F_{Dex}^{D} the donor fluorescence intensity D after donor excitation Dex, F_{Aex}^{A} the acceptor fluorescence intensity A after acceptor excitation Aex, l is the leakage factor determined from the donor only population, d the direct excitation factor determined from the acceptor only population, Q the quantum efficiency of the respective dye, and η efficiency of the respective detector.

Using the same correction factors the stoichiometry is defined by:

$$S = \frac{\gamma F^{D}_{Dex} + F^{A}_{Dex} - lF^{D}_{Dex} - dF^{A}_{Aex}}{\gamma F^{D}_{Dex} + F^{A}_{Dex} - lF^{D}_{Dex} - dF^{A}_{Aex} + F^{A}_{Aex}} \quad (9)$$

For quantification of the low FRET and the high FRET populations we assume a FRET efficiency threshold of 0.4.

TIRF FRET Setup & Procedures

Setup

To monitor dynamics of N-terminal opening and closing single molecule total internal reflection (TIR) FRET studies were performed using a custom build prism-type internal reflection fluorescence microscope similar to the one previously described in (4). The sample was illuminated by a green laser (532 nm Compass 215 M 75 mW Coherent Inc, USA) with approximately 1 mW. Fluorescence light of the donor and acceptor was collected by an apo TIRF 60x 1.49na (Nikon, Japan) objective, separated and recorded on two Andor DV887 (Andor Technology, UK) cameras.

Preparation

Proteins were labeled and exchanged like in the confocal FRET setup section, except that the acceptor molecule was non-specifically biotinylated (with NHS-PEG-Biotin) for surface immobilization as described in (4) after dye labeling.

Measurement Procedure and Evaluation

25 pM heterodimers were incubated on self-prepared PEG Streptavidin quartz glass slides. Unbound sample was washed out with measurement buffer (see optical trap procedures). Measurement interval was 220 ms (200 ms illumination and 20 ms camera readout). Measurements were carried out at 30°C. Time traces of the donor and acceptor signal were extracted from the recorded image stack. FRET efficiencies were corrected for direct excitation and leakage. FRET efficiencies were smoothed (sliding average of 5 frames) and pooled in histograms.

Biochemical methods

Crosslinking Experiments

To check the influence of the CL flexibility in the N-terminal closed state, crosslinking experiments were performed with zipped Hsp90 constructs (WTzip, Sub211-263zip and Sub211-272zip) carrying the cysteine mutation at position 61. Prior to crosslinking, proteins were reduced with 10mM TCEP and buffer was exchanged to PBS pH 6.7.

10 µM of cysteine specific crosslinking agent $BM(PEG)_3$ (1,11-bis(maleimido)triethylene glycol, Thermo Scientific, USA) were mixed with 3 µM Hsp90 and incubated at room

temperature (about 25°C) for 15 minutes. The reaction was quenched with an excess of DTT (dithiothreitol).

Cross-linked samples were separated on a reduction free 10% SDS-PAGE.

ATPase assay

ATPase assays were performed using an ATP regenerating system (17, 18). Hsp90 concentrations were 3 µM and the assays were measured in 40 mM Hepes, 150 mM KCl, 5 mM $MgCl_2$ at 30°C. To subtract the background activity, radicicol was added at the end of the measurement. The data was analyzed by linear regression and in case of chaperone titrations fitted according to Michaelis-Menten equation. For the activation by Aha1, the Hsp90 concentration was reduced to 1 µM and a low salt assay buffer (40 mM Hepes, 20 mM KCl, 5 mM $MgCl_2$ pH 7.5) was used (19).

The absolute ATPase activity measured for WT shown in Figure 4C was 0.36 ± 0.01 min^{-1}.

In vivo methods

Yeast Methods and Plasmid shuffling

Standard methods for growth and transformations were employed. All in vivo experiments were measured as triplicates of independent clones. Cells were cultured on selective minimal medium (0.67 % yeast nitrogen base, 2 % glucose and amino acids depending on auxotrophy) at 30°C. To introduce the linker mutants into yeast as the only source of Hsp90 a plasmid shuffling approach was used (20). To this end, the linker substitution mutants were cloned into p423GPD vectors (ATCC, USA) and transformed in the yeast strains ECU82α (21) or ECU82α lacking Cpr7, whose only copies of Hsp90 reside on a URA3-containing pKAT6 plasmid. The co-transformants were cultivated on -HIS/-LEU plates and 5-FOA was used to select for positive clones.

Stress assays

Overnight cultures were adjusted to an OD_{600} of 0.5 and 1:5 dilutions were spotted onto selective agar plates. The growth of the different yeast strains was compared after 48 h. To test the influence of Hsp90 in nucleotide excision repair (NER), the spotted plates were exposed to UV light (40 J/m^2 and 80 J/m^2) at room temperature and afterwards incubated for 48 h at 30°C.

GR assay

A sensitive readout for Hsp90 function *in vivo* is the activity of the mammalian glucocorticoid receptor (GR) receptor (21). To assess the impact of the linker replacements on the chaperoning of GR, yeast cells were transformed with a plasmid constitutively expressing GR. Positive clones were cultivated overnight in selective medium and diluted into medium containing 10 µM desoxycorticosteron for approx. 12 h. As activated GR binds to a response element coupled to the *lacZ* gene, the expression of β-galactosidase can be used as an indirect readout for GR activity. To monitor β-galactosidase activity, cells were lysed and its substrate ONPG (o-nitrophenyl β-D-galactopyranoside, Sigma) was added. Formation of the chromogenic substrate ortho-nitrophenol was monitored at 405 nm in a Tecan plate reader and for data comparison corrected by the optical density (OD_{600}) of the samples.

v-src kinase assay

The viral tyrosine kinase v-src is another Hsp90 client protein (21). To test the ability of the linker mutants to activate this protein, a plasmid carrying v-src kinase under the inducible Gal promoter was transformed in yeast cells. Cells were grown for two days in raffinose-containing medium before they were adjusted to an OD_{600} of 0.5 and spotted in 1:5 dilutions onto glucose and galactose containing plates. The growth of the yeast was analyzed after 48 h at 30°C. To monitor the phosphotyrosine levels by Western Blot analysis, v-src expression was induced for 6 h at 30°C.

Immunoblotting

Cells were harvested and total cell extract was obtained by using an alkali treatment (22). Equal amounts of protein were separated by electrophoresis through SDS-PAGE and transferred onto a PDVF-membrane. The Western Blot was blocked with 5 % milk powder in TBS-T overnight and afterwards incubated with the primary antibody. A horseradish peroxidase-conjugated secondary antibody was used to detect the antigen-antibody interaction by chemiluminescence.

Analytical Ultracentrifugation

To analyze the ability to form complexes with cochaperones, the Hsp90 mutants were subjected to analytical ultracentrifugation with a fluorescence detection system (Beckman/Coulter, USA and Aviv, USA). Therefore labeled cochaperones (0.5 µM Aha1-FAM, 1 µM Sba1/p23-Atto488, 1 µM Sti1-Atto550) were incubated in the absence (Aha1) or presence of 2 mM AMP-PNP (Sba1/p23) with 3 µM of Hsp90 WT or mutants. Buffers were the same as for the ATPase assay. Runs were performed at 42000 rpm and 20 °C. The raw data were analyzed using the program Sedview (23) and obtained dc/dt curves were fitted with Gaussian functions.

SI Figures

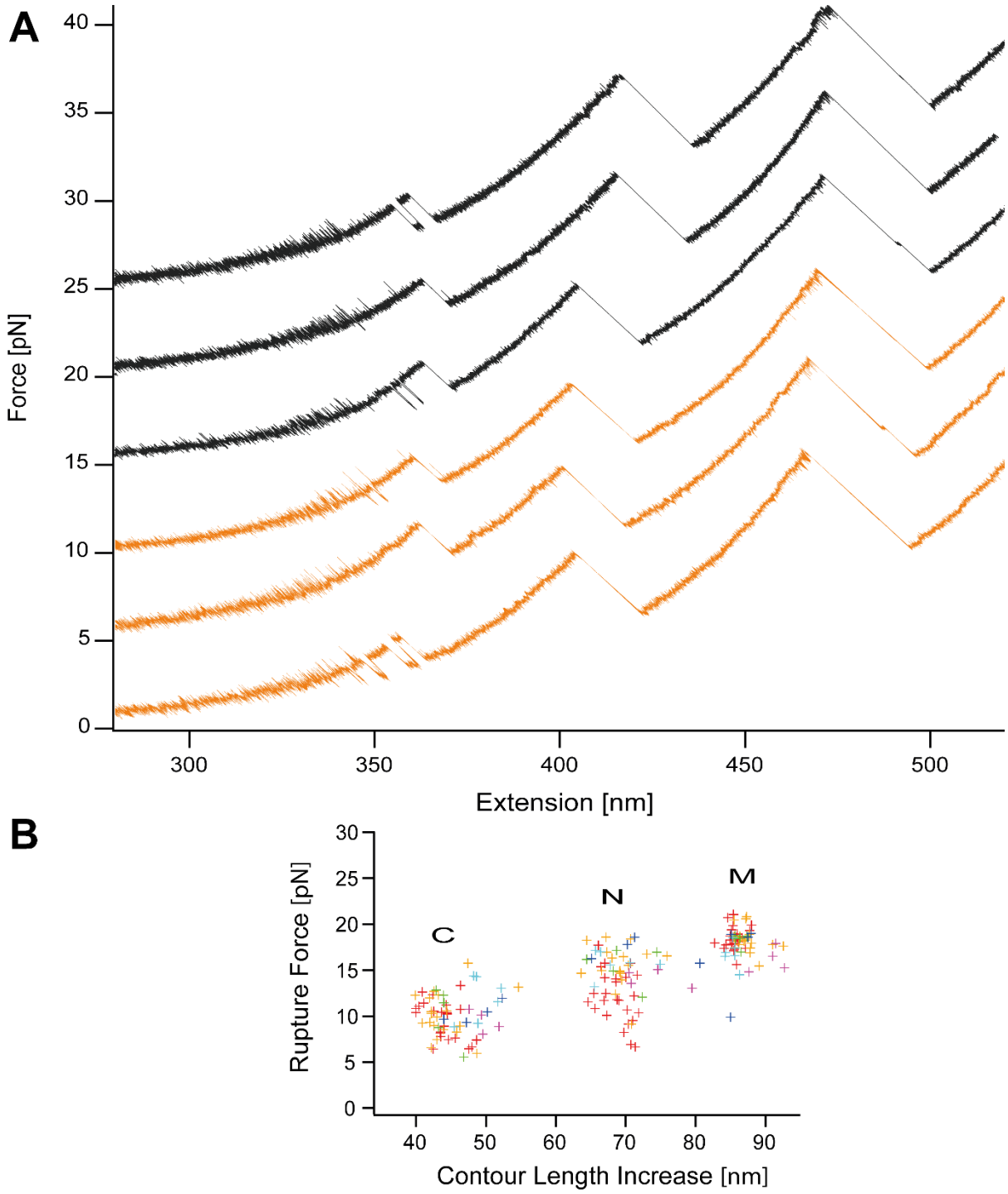

Figure S1: Force-extension traces and scatter plot of Hsp90

(A) Force-extension curves of Hsp90 (WT-diUbi) from individual experiments with a pulling velocity of 10 nm/s show the reproducibility of Hsp90's unfolding pattern. Black traces were measured with the standard scavenger system described in the methods section. The same unfolding pattern was observed (orange traces) using Trolox (6-hydroxy-2,5,7,8-tetramethylchroman-2-carboxylic acid, Sigma, Germany) as scavenger. Traces are offsetted by 5 pN for clarity.

(B) Each domain unfolding event can be associated with a rupture force and a contour length gain. The rupture forces of multiple molecules from different individual molecules (color-coded) are plotted against their associated contour length gains. Each point represents one unfolding event. Three distinct population representing the N-, M- and C-domain are observed. Rupture forces are higher than in (A) due to a different pulling speed of 500 nm/s.

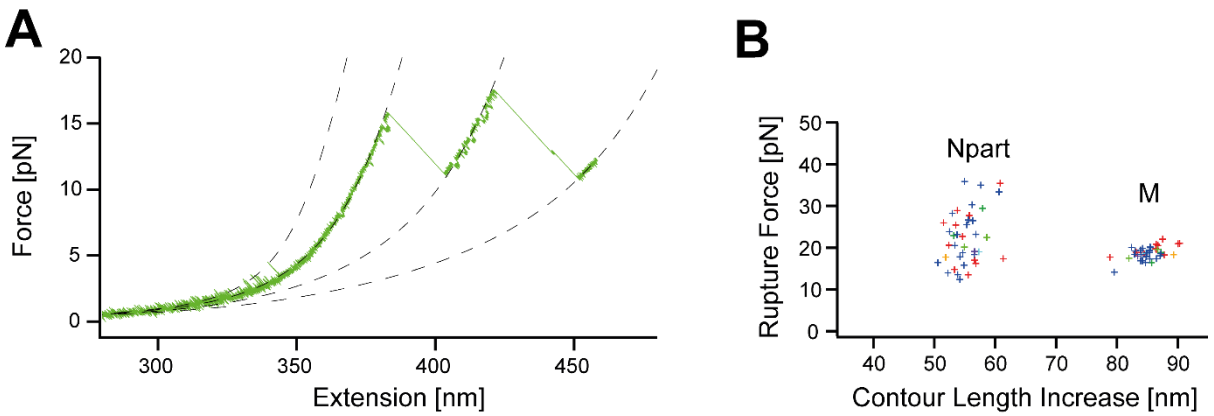

Figure S2: Force-extension trace and scatter plot of Hsp90 with internal cysteines

(A) Filtered full length force-extension curve (10 nm/s) of Hsp90 (WT_cys) with WLC fits (dashed) to the individual domains. To exclude effects of ubiquitins and increase resolution the force was applied on the amino acid positions 61 and 560, thus a shortened N domain and no C domain is observed.

(B) Scatter Plot of rupture forces against contour length increases of Hsp90 (WT_cys) as described in Fig. S1B. The shortened N-domain (Npart) and the middle domain (M) are observed.

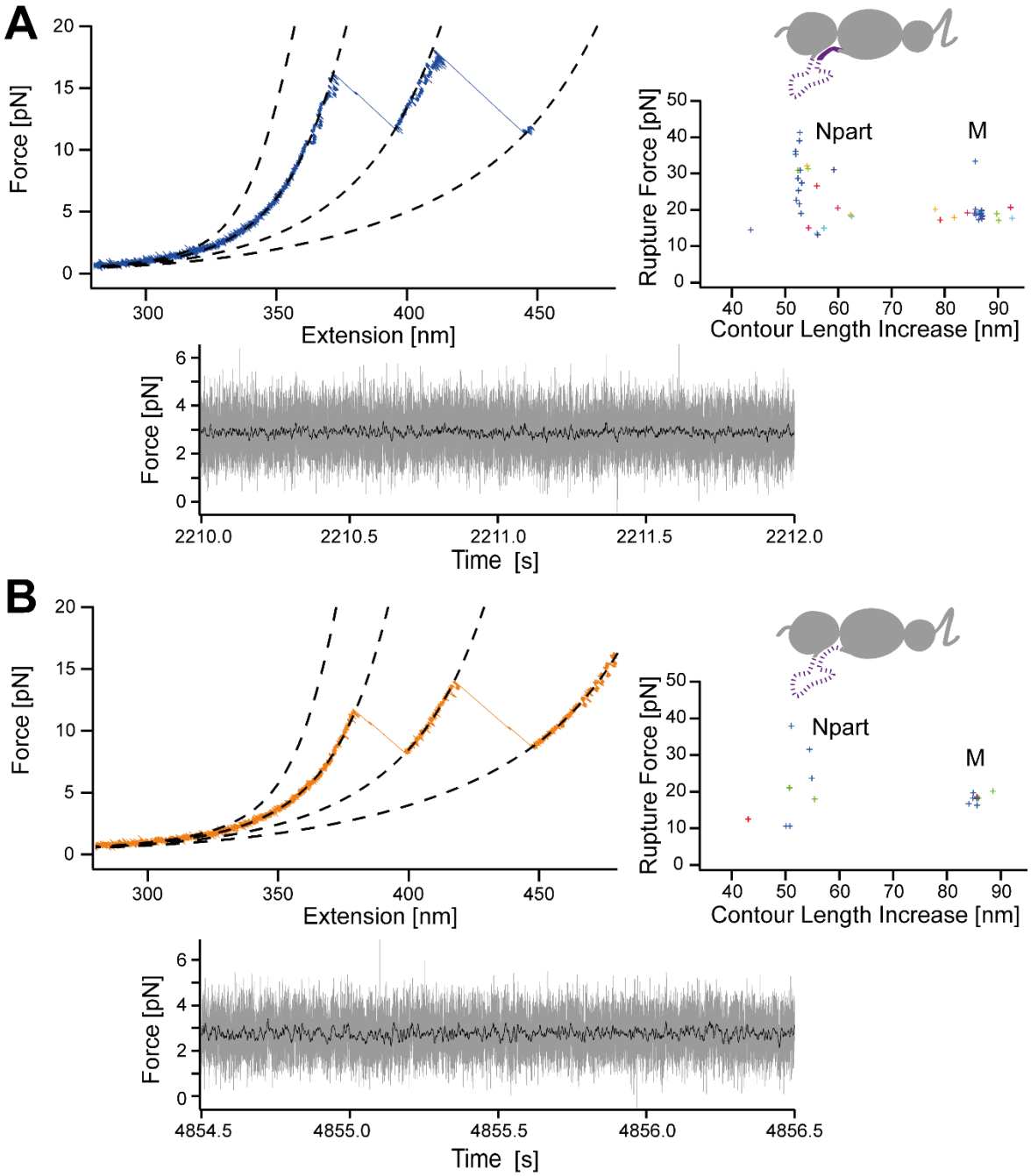

Figure S3: Force-extension traces, scatter plots and constant distance traces of substitution constructs

(A) Full length trace of Sub211-263 with WLC fits (A, top left). The unfolding pattern is identical to the one observed in Hsp90 (WT_cys in Fig. S2) with the exception that the CL is not observed. A scatter plot of Sub211-263 is depicted (A, top right) as well as a segment of a constant distance trace (A, bottom). (B) Same experiments with identical results are shown for Sub211-272.

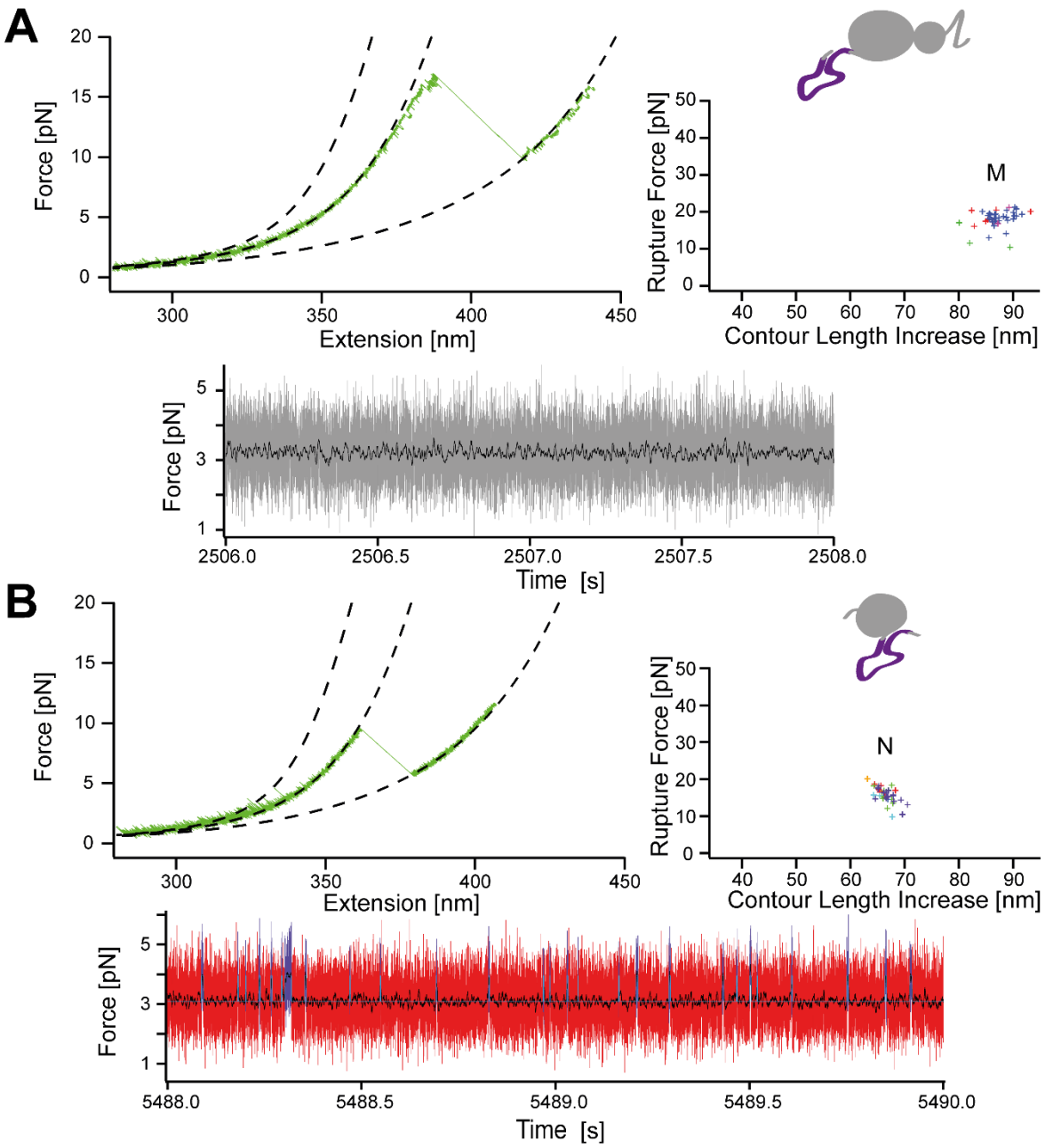

Figure S4: Force-extension traces, scatter plots and constant distance traces of deletion constructs

(A) Full length trace of Hsp90 WT-ΔN with WLC fits (A, top left). The CL docked state is not observed if the N domain is deleted. A scatter plot of Hsp90 WT-ΔN is depicted (A, top right) as well as a segment of a constant distance trace (A, bottom). (B) Same experiments are shown for Hsp90 WT-ΔMC. If the N domain is present the docked state of the CL is observed in force-extension curves and constant distance traces.

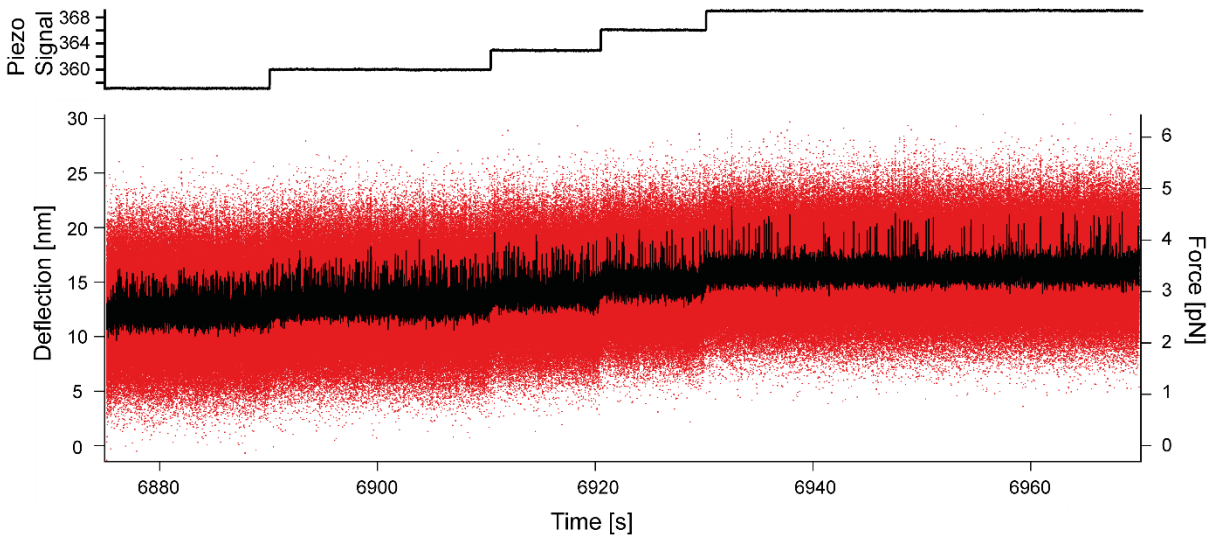

Figure S5: Full length constant distance experiment of WT_cys.

Top graph shows the signal of the movable piezo mirror over time. It is related to the bead-bead distance and a higher signal corresponds to a higher average force. This is visible in the force trace (bottom). Red trace is unfiltered data. The filtered data (black) clearly shows the increase in average force as well as the shift in CL kinetics to the undocked conformation. In our setup we can observe a single molecule for several minutes.

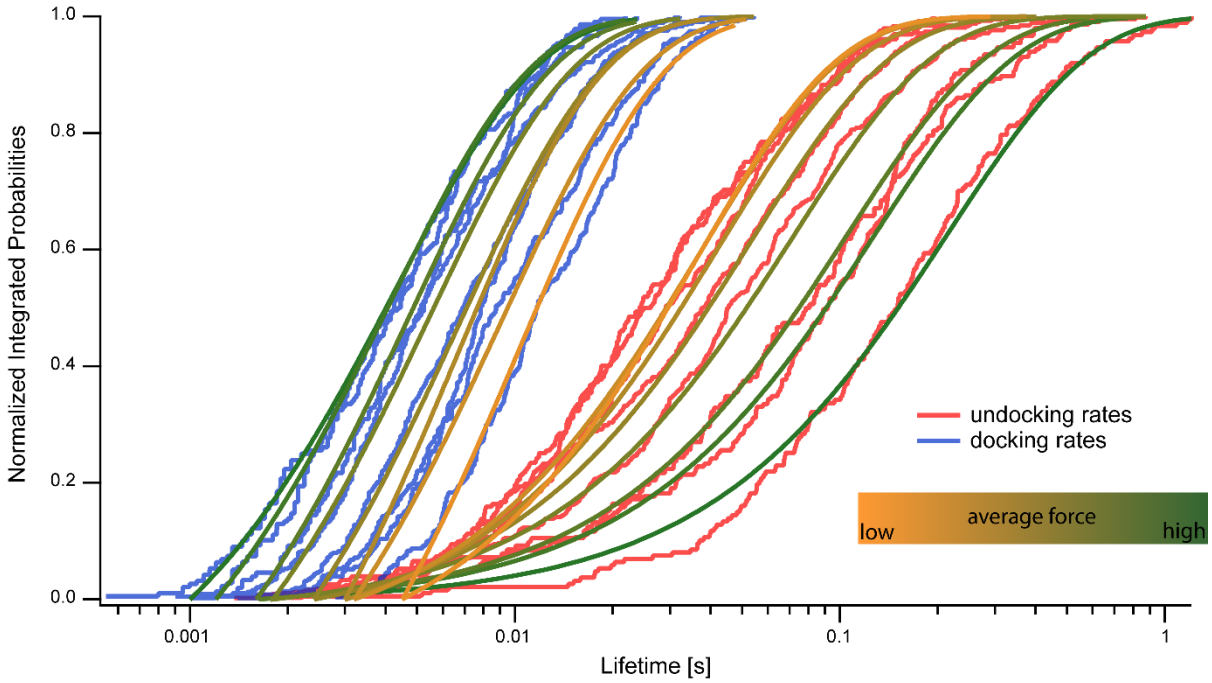

Figure S6: Derivation of rate constants at different average forces from a single molecule.

Integrated Lifetime Histograms of the sample experiment in Figure 3 of undocking (blue) and docking (red) at different average forces. Histograms are fitted with single exponential fits with a cut off for not detected fast transitions. Color-coded is the average applied force for each docking and undocking pair. As expected, undocking rates increase with increasing average force (orange to green), docking rates behave the opposite way.

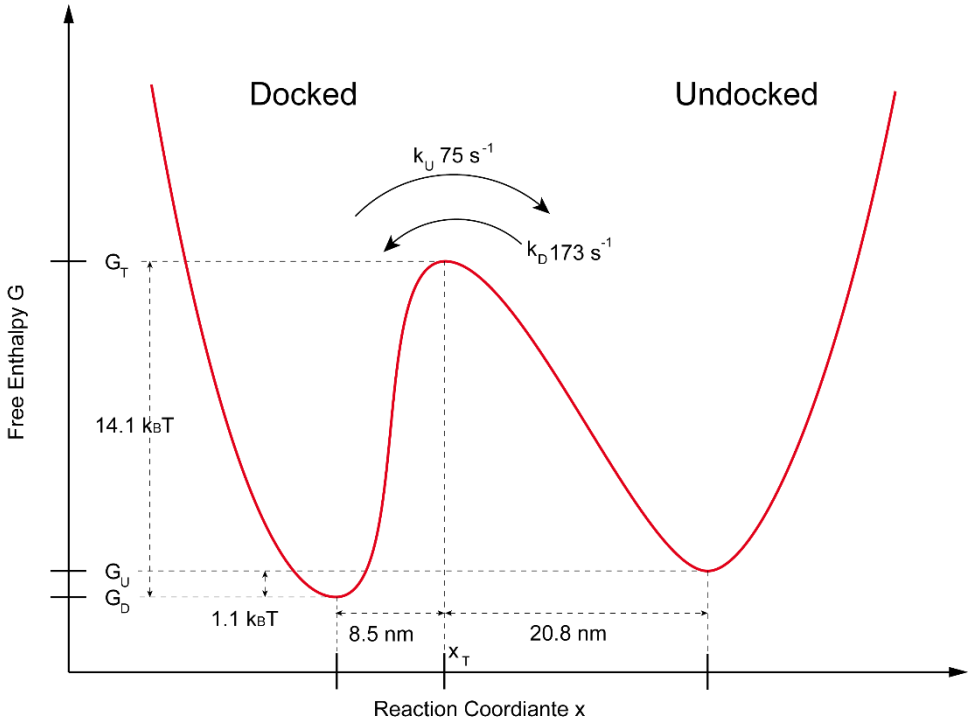

Figure S7: Schematic energy landscape of the charged linker

The energy landscape between the docked state and the undocked state along the reaction coordinate x. The energy difference $|G_u - G_d|$ between the docked and the undocked state is 1.1 k_BT. The height of the energy barrier $|G_T|$ was estimated using Arrhenius equation for the undocking rate k_u with an attempt frequency of 10^8 s^{-1}. The positions of the transition state along the reaction coordinate from the docked or undocked state are derived from the force dependent rate fits (see methods equation 6). The distance between docked and undocked state is approximately 29.3 nm and corresponds well with the length observed in constant velocity experiments.

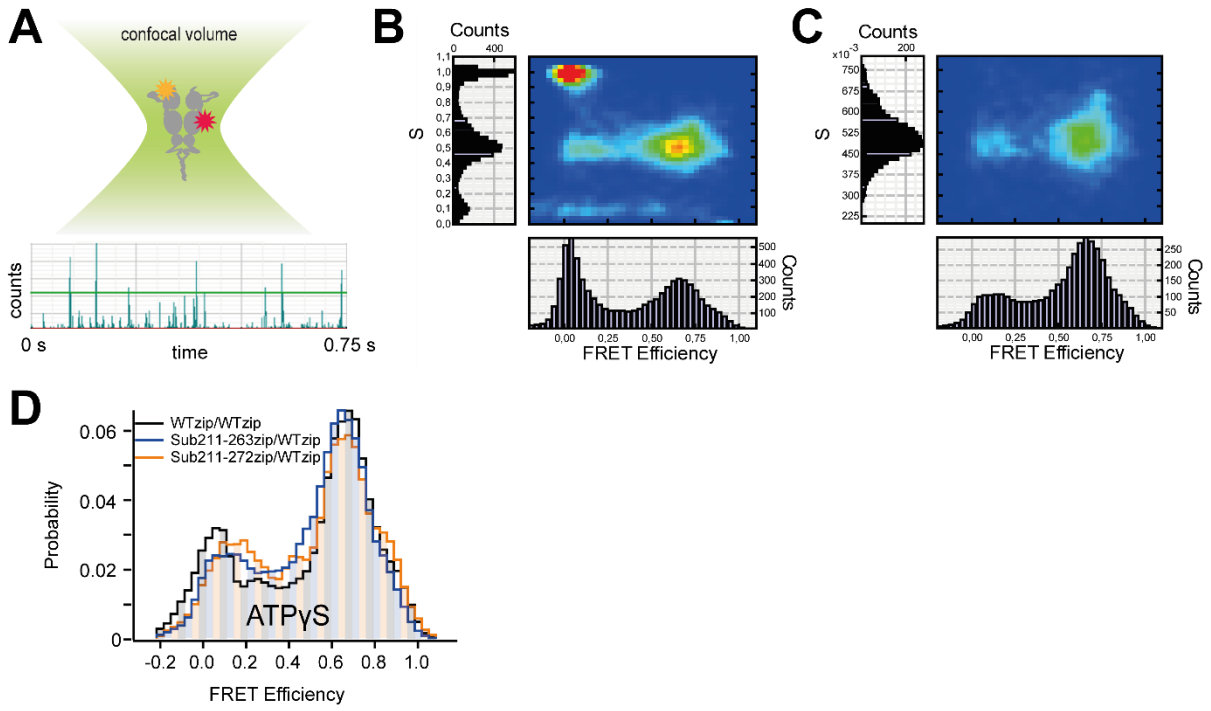

Figure S8: Evaluation of sm confocal FRET experiments and histograms with ATPγS

Hsp90 dimers are allowed to diffuse through a confocal spot (A) and fluorescent light in the donor and acceptor channel is observed over time. Every time a fluorescent molecule is within the confocal volume a fluorescence burst (total intensity) is measured. Bursts exceeding a certain threshold (green line) are collected in 2-D histograms (B). On the y-axis the stoichiometry S (see methods equation 9) and on the x-axis the FRET efficiency (see methods equation 7) is plotted. Selecting for a stoichiometry of around 0.5, we obtain the FRET histograms shown in (C). The shown data is from experiments with Sub211-272zip/WTzip with 2 mM ATPγS. (D) Histograms of WT and CL mutants preincubated with ATPγS. (compare to Figure 4A)

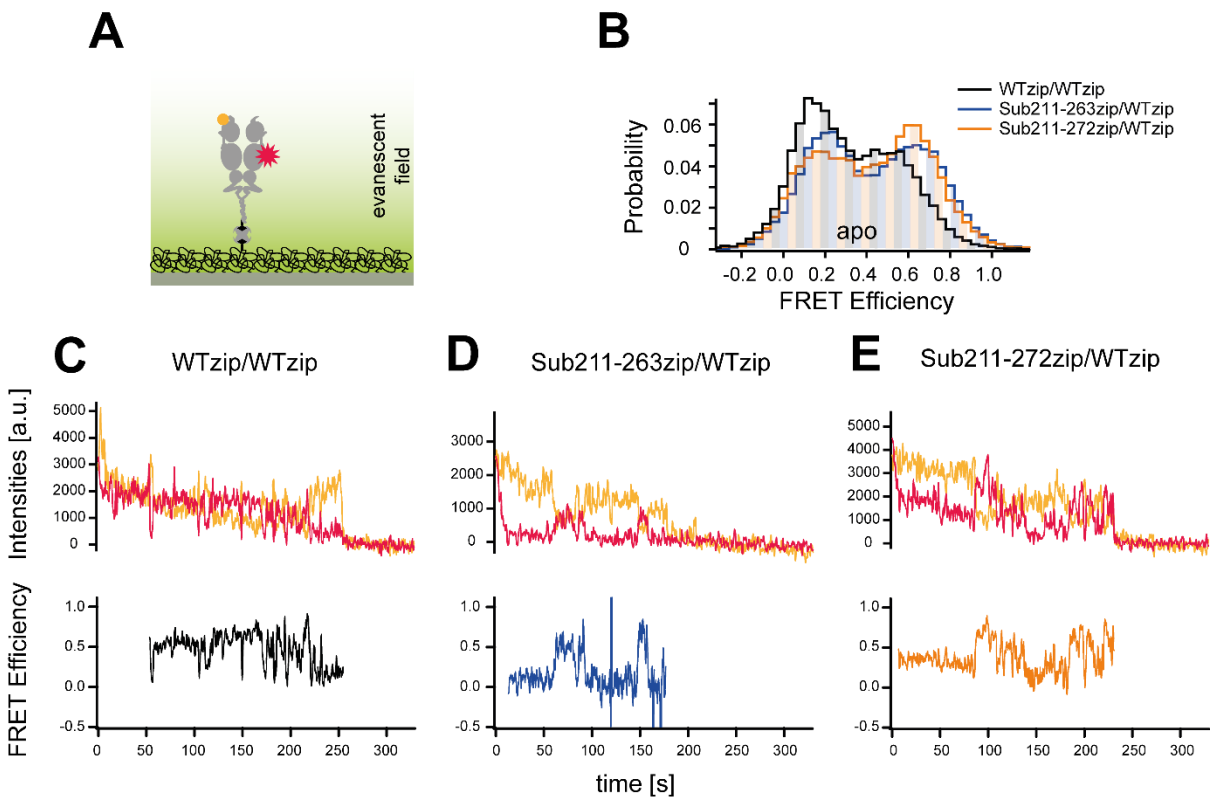

Figure S9: Single molecule TIR-FRET

(A) Schematics of the TIR-FRET experiment. Hsp90 hetero-dimers are immobilized via biotin-streptavidin and their FRET efficiency is monitored over time. (B) Histograms of FRET efficiencies for the apo state. Each histogram contains a minimum of 34 individual molecules and over 21213 data points.

Example Traces of sm TIR-FRET of a WT_zip/WT_zip FRET pair (C), a Sub211-263zip/WT_zip FRET pair (D) and a Sub211-272zip/WT_zip FRET pair (E). Top graphs show fluorescent intensities over time of donor (orange) and acceptor (red). Bottom graphs show the calculated FRET efficiencies from intensity traces. All constructs show opening/closing dynamics.

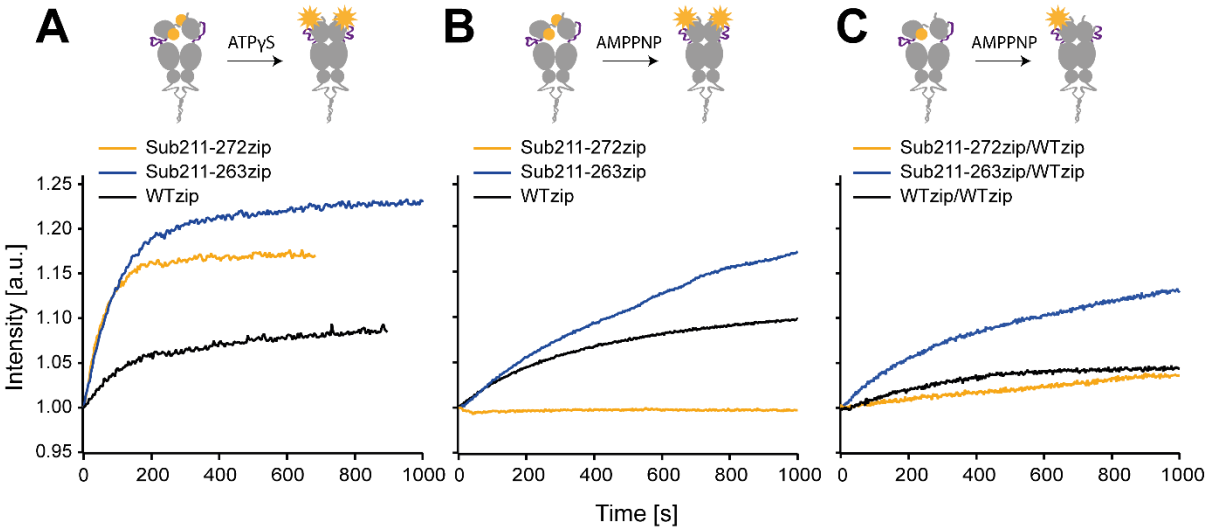

Figure S10: Fluorescence experiments with ATPγS and AMP-PNP

Upon the addition of ATPγS (A) or AMP-PNP (B,C) Hsp90 is shifted into a closed and compact conformation. The fluorescence signal of labeled Hsp90 is increased (de-quenched) in this conformation. This is due to some quenching in the non-compact state. Homodimers of WTzip (black), Sub211-263zip (blue) and Sub211-272zip (yellow) were labeled with Atto550 (at aa position 61) and their fluorescence is monitored over time after the addition of ATPγS (A). Substitution mutants show increased fluorescence recovery suggesting that the orientational freedom leads to increased quenching (and therefore increased de-quenching upon the addition of nucleotide). (B) Addition of AMPPNP leads to a similar behavior except for Sub211-272zip that is not influenced by AMPPNP at all. (C) This behavior can be partially rescued if one monomer is substituted with WT_zip (10 fold excess).

All intensity traces have been normalized to 1 upon addition of nucleotide. Experiments were performed on a Jasco FP-8500 spectrofluorimeter (Germany) exciting 500 nM labeled protein at 530 nm and measuring its emission at 580 nm. All constructs were measured multiple times each time showing identical behavior.

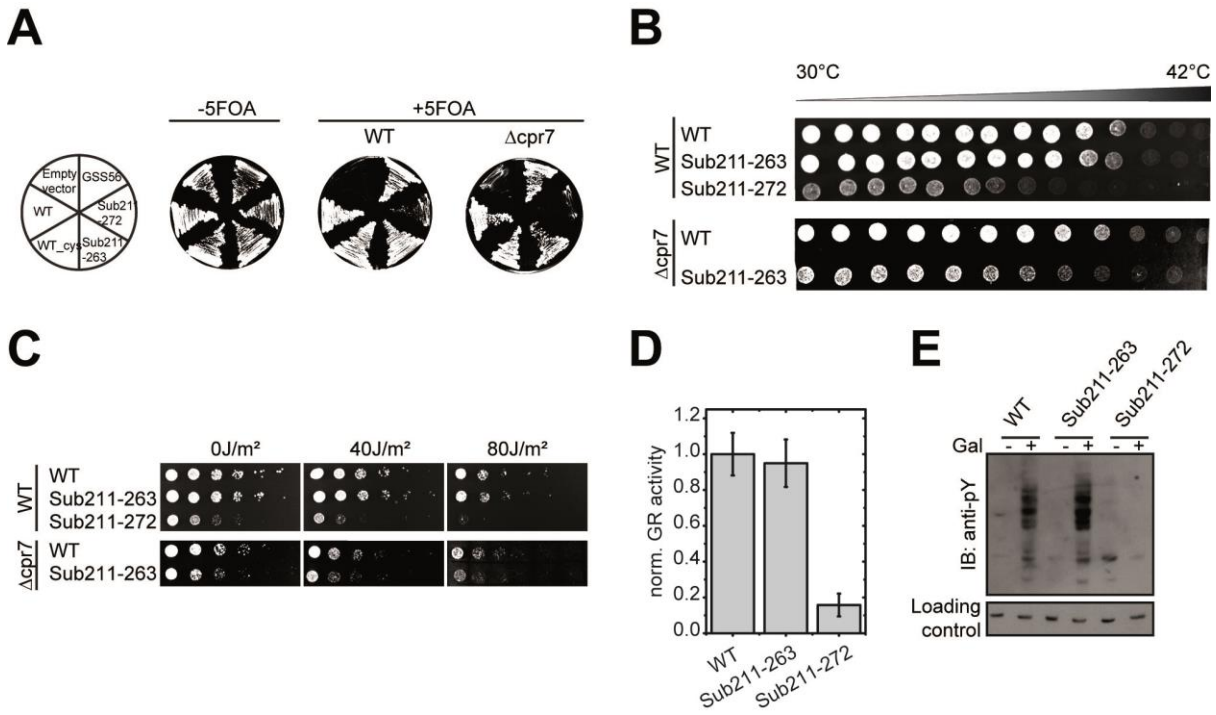

Figure S11: Invivo effects of the substitution mutants

(A) A FOA-shuffling approach was used to introduce the Hsp90 variants as the sole source of Hsp90 in the cell. (B) Analysis of the temperature-dependent growth of the WT and the substitution mutants. (C) Substitution mutants were tested towards their sensitivity against UV light. (D) The activity of the steroid hormone receptor GR was measured using a ß-galactosidase-coupled reporter assay. (E) Analysis of the linker substitution mutants on the Hsp90 client v-src. Immunoblots show hyperphosphorylation due to active v-src kinase.

SI Tables & Comments

Construct	Domain N [nm]	Domain M [nm]	Domain C [nm]	Traces/Molecules
WT-diUbi	68.41+-2.07	85.38+-1.02	42.89+-2.33	69 / 6
WT_cys	53.73+-1.48	85.56+-1.37		46 / 13
WT_ΔN		85.63+-1.80		51 / 4
WT_ΔMC	66.00+-1.40			39 / 6
Sub211-263	54.45+-3.81	86.26+-3.25		26 / 7
Sub211-272	51.47+-3.53	86.00+-1.43		10 / 3

Table S1: Contour length increases of Hsp90's domains for all shown constructs.

Cells are blank if the domain is not observed due to deletion or pulling geometry. In WT_cys, Sub211-263 and Sub211-272 the N domain is only partially unfolded because force is applied within the N domain (aa 61). Within error all data is self-consistent, implying no major domain disruptions by substituting the CL or cysteine mutations. Last row states the number of force extension traces evaluated and the number of individual molecules. Mean values and standard deviation (sd) were derived from Gaussian fits. For Sub211-263 and Sub211-272 arithmetic mean and sd were used.

Construct	Domain N [pN]	Domain M [pN]	Domain C [pN]	Traces/Molecules
WT-diUbi	14.05+-1.90	17.63+-0.59	9.20+-1.74	62 / 6
WT_cys	20.24+-4.77	17.61+-1.04		39 / 13
WT_ΔN		17.86+-1.13		44 / 4
WT_ΔMC	15.40+-1.22			28 / 6
Sub211-263	24.31+-9.71	18.60+-4.94		24 / 7
Sub211-272	18.43+-11.62	16.22+-6.21		8 / 3

Table S2: Rupture forces at constant velocity (500nm/s) of Hsp90's domains for all shown constructs.

Cells are blank if the domain is not observed due to deletion or pulling geometry. If force is applied at aa position 61 in the N-terminal domain (WT_cys, Sub211-263 and Sub211-272) forces are increased and the distribution broadened due to the different force exertion point. Within error all data is self-consistent, implying no major domain disruptions by substituting the CL or cysteine mutations. Last row states the number of traces evaluated and the number of individual molecules. Mean values and standard deviation were derived from Gaussian fits. For Sub211-263 and Sub211-272 arithmetic mean and sd were used.

Domain (amino acid region)	Distance from crystal structure [nm]	Expected Length Gain [nm]	Measured Length Gain [nm]
N domain (2-208)	6.52	69.04	68.41+-2.07
Part of N domain (61-208)	1.64	52.38	53.73+-1.48
M domain (273-527)	6.54	86.53	85.38+-1.02
C domain (528-709)	4.57 (assumed)	61.86	42.89+-2.33
Folded C domain (538-671)	3.87	45.04	42.89+-2.33

Table S3: Measured and Expected Length Gains of Hsp90's Domains.

The measured contour length increases of WT-diUbi and WT_cys (Table S1 & S2) are compared to the theoretical values calculated from crystal structure (see methods equation 3). Values calculated agree well with measured domain sizes. The last two rows show that the C terminal domain is not completely folded as already suggested by the crystal structure. Assuming that the folded part is aa 538 to 671, as in the crystal structure the expected contour length increase fits the measured well.

Comment S1: CL Contour Length

The measured CL length in constant distance experiments is around 32 nm. Distances from and to the transition state sum up to 29 nm (see energy landscape Fig. S7). In constant velocity experiments CL length of about 28 nm results in best fits. From its length of 62 aa we would expect an unfolding length of 22.6 nm minus the initial distance of 2.3 nm between aa 211 and 272 given by the crystal structure. All other domains show good agreement with theoretical values but the measured CL length is approximately 8 nm too long. The most likely reason for this difference is the charged nature of the CL. It contains 28 negatively charged and 18 positively charged residues. Highly charged polypeptides are known to have an increased persistence length (24) which in turn lead to a lower contour length gain especially at low forces. For example assuming a persistence length of 1.3 nm instead of 0.7 nm we get 21.9 nm instead of 34.3 nm. Another additional reason might be that undocking forces a rotation of domains against each other. That could account for up to 4 nm. However the effect of variations in persistence and contour lengths on calculated energies and rates is very limited (less than 10%), because persistence length and contour length increase cancel.

References

1. Stigler, J., Ziegler, F., Gieseke, A., Gebhardt, J. C. M. & Rief, M. (2011) *Science* **334,** 512-516.
2. Rognoni, L., Stigler, J., Pelz, B., Ylanne, J. & Rief, M. (2012) *Proceedings of the National Academy of Sciences of the United States of America* **109,** 19679-19684.
3. Panavas, T., Sanders, C. & Butt, T. (2009) in *SUMO Protocols SE - 20*, ed. Ulrich, H. D.-.-.-.-.-. (Humana Press DA - 2009/01/01, pp. 303-317.
4. Mickler, M., Hessling, M., Ratzke, C., Buchner, J. & Hugel, T. (2009) *Nature Structural & Molecular Biology* **16,** 281-286.
5. Buchner, J., Weikl, T., Bugl, H., Pirkl, F. & Bose, S. (1998) *Molecular Chaperones* **290,** 418-429.
6. Retzlaff, M., Hagn, F., Mitschke, L., Hessling, M., Gugel, F., Kessler, H., Richter, K. & Buchner, J. (2010) *Molecular Cell* **37,** 344-354.
7. von Hansen, Y., Mehlich, A., Pelz, B., Rief, M. & Netz, R. R. (2012) *Review of Scientific Instruments* **83**.
8. Cecconi, C., Shank, E. A., Bustamante, C. & Marqusee, S. (2005) *Science* **309,** 2057-2060.
9. Wang, M. D., Yin, H., Landick, R., Gelles, J. & Block, S. M. (1997) *Biophysical Journal* **72,** 1335-1346.
10. Rabiner, L. (1989) *Proceedings of the IEEE* **77,** 257-286.
11. Heinrich, F., Ng, T., Vanderah, D. J., Shekhar, P., Mihailescu, M., Nanda, H. & Losche, M. (2009) *Langmuir* **25,** 4219-29.
12. Stigler, J. & Rief, M. (2012) *Chemphyschem* **13,** 1079-1086.
13. Kapanidis, A. N., Laurence, T. A., Lee, N. K., Margeat, E., Kong, X. & Weiss, S. (2005) *Acc Chem Res* **38,** 523-33.
14. Müller, B. K., Zaychikov, E., Brauchle, C. & Lamb, D. C. (2005) *Biophys J* **89,** 3508-22.
15. Kudryavtsev, V., Sikor, M., Kalinin, S., Mokranjac, D., Seidel, C. A. & Lamb, D. C. (2012) *Chemphyschem* **13,** 1060-78.
16. Ratzke, C., Berkemeier, F. & Hugel, T. (2012) *Proceedings of the National Academy of Sciences of the United States of America* **109,** 161-166.
17. Tamura, J. K. & Gellert, M. (1990) *Journal of Biological Chemistry* **265** 21342-9
18. Panaretou, B., Prodromou, C., Roe, S. M., O'Brien, R., Ladbury, J. E., Piper, P. W. & Pearl, L. H. (1998) *Embo Journal* **17,** 4829-4836.
19. Panaretou, B., Siligardi, G., Meyer, P., Maloney, A., Sullivan, J. K., Singh, S., Millson, S. H., Clarke, P. A., Naaby-Hansen, S., Stein, R., Cramer, R., Mollapour, M., Workman, P., Piper, P. W., Pearl, L. H. & Prodromou, C. (2002) *Molecular Cell* **10,** 1307-1318.
20. Sikorski, R. S. & Boeke, J. D. (1991) *Methods in Enzymology* **194,** 302-318.
21. Nathan, D. F. & Lindquist, S. (1995) *Molecular and Cellular Biology* **15,** 3917-3925.
22. Kushnirov, V. V. (2000) *Yeast* **16,** 857-860.
23. Hayes, D. B. & Stafford, W. F. (2010) *Macromol Biosci* **10,** 731-5.
24. Leake, M. C., Wilson, D., Gautel, M. & Simmons, R. M. (2004) *Biophys J* **87,** 1112-35.